ORIGINAL ARTICLE

lajss.org© Latin American Journal of Solids and Structures

www.lajss.org

Influence of Radial Stiffness of Surrounding Rock on Dynamic Behaviour of End-anchored Rockbolt under Impact Loading

Xingzhong Wu[a], Yubao Zhang[a,b]*, Zijian Zhang[a], Minglu Xing[a,b], Jianye Fu[a], Longhai Li[a], Pengfei Liu[c]

[a]College of Energy and Mining Engineering, Shandong University of Science and Technology, Qingdao, Shandong, China. Email: 2287985304@qq.com, yubao.zhang@sdust.edu.cn, 250925192@qq.com, sixingziwei@163.com, 1257804732@qq.com, 979325061@qq.com

[b]State Key Laboratory of Mining Disaster Prevention and Control Co-founded by Shandong Province and the Ministry of Science and Technology, Shandong University of Science and Technology, Qingdao, Shandong, China .

[c]Ningxia Hongdunzi Coal Industry Co., Ltd, Yinchuan, Ningxia Hui Autonomous Region, China. Email: 123378774@qq.com

*Corresponding author

https://doi.org/10.1590/1679-78258137

Abstract

The surrounding rock stiffness has a significant effect on the impact mechanical properties of rockbolts. In order to study the influence of radial stiffness of surrounding rock on the dynamic characteristics of the end-anchored rockbolt, numerical simulations of drop weight impact tests on the end-anchored rockbolt were conducted using finite element method. The simulation results show that the larger the radial stiffness of the surrounding rock, the larger the value of the absorbed impact energy of end-anchored rockbolt. However, there is an upper limit to the effect of radial stiffness on the dynamic behavior of end-anchored rockbolt, i.e., the value of absorbed impact energy tends to be stabilized when the radial stiffness exceeds 2.91 GPa/mm. In the impact simulation, the fracture position of the bolt bar is affected by both radial stiffness and impact energy. The greater the radial stiffness of the surrounding rock, the further the fracture location is away from the anchorage end. The larger the impact energy is, the closer the fracture location is to the anchorage end. It is important to study and determine the range of fracture location of anchor rods to develop new types of anchor rods and to design the support scheme for the surrounding rock under dynamic loading. Finally, due to the linkage between numerical simulation and indoor tests, the effect of steel pipe wall thickness on the upper and lower limits of the results also provides a theoretical basis for the rationalization of the design of steel pipe wall thickness. The study of dynamic impact fracture location of bolt bar is of great significance for the development and design of new types of rockbolt under dynamic loading.

Keywords

End-anchored rockbolt, radial stiffness, dynamic response, energy absorption, bolt fracture position

Graphical Abstract

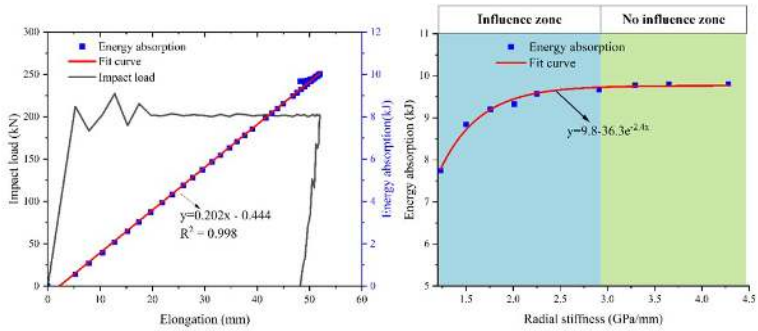

Received: mar. 31, 2024. In revised form: jul. 11, 2024. Accepted: ago. 19, 2024. Available online: ago. 20, 2024.
https://doi.org/10.1590/1679-78258137

Latin American Journal of Solids and Structures. ISSN 1679-7825. Copyright © 2024. This is an Open Access article distributed under the terms of the Creative Commons Attribution License, which permits unrestricted use, distribution, and reproduction in any medium, provided the original work is properly cited.

1 INTRODUCTION

At present, rockbolt is the most widely used, economical, and convenient means of rock support in underground mining and tunneling projects (Ren et al. 2010; Li et al. 2016; Zhao et al. 2021a). There are various types of rockbolt including mechanical bolt, grouted bolt, yield bolt, etc., among which end-anchored rockbolt is the most commonly used in coal mining in China (Zhao et al. 2021; Knox and Hadigeorgiou 2023). As shown in Figure 1, the schematic diagram of the end-anchored rockbolt structure is shown. With the gradual increase of coal mining depth, large deformation of surrounding rock and rock burst caused by high ground stress occur frequently. The traditional static rockbolt reinforcement theory based on the strength of the surrounding rock is difficult to be applied to the complex and variable dynamic load environment. Researchers have studied the interaction between surrounding rock and rockbolt under dynamic load through a large number of field investigations, laboratory tests and theoretical analysis methods. Some yield rockbolts with impact resistance that can adapt to the large deformation of surrounding rock and absorb energy have been developed. For example, the D-bolt, invented by Li (2010), is a multi-point anchoring structure that maximizes the strength and deformation capacity of the entire bolt length. The NPR rockbolt, developed by He et al. (2022), has a strong tensile capacity, high constant resistance, and an ideal elastic-plastic constitutive model with a negative Poisson's ratio.

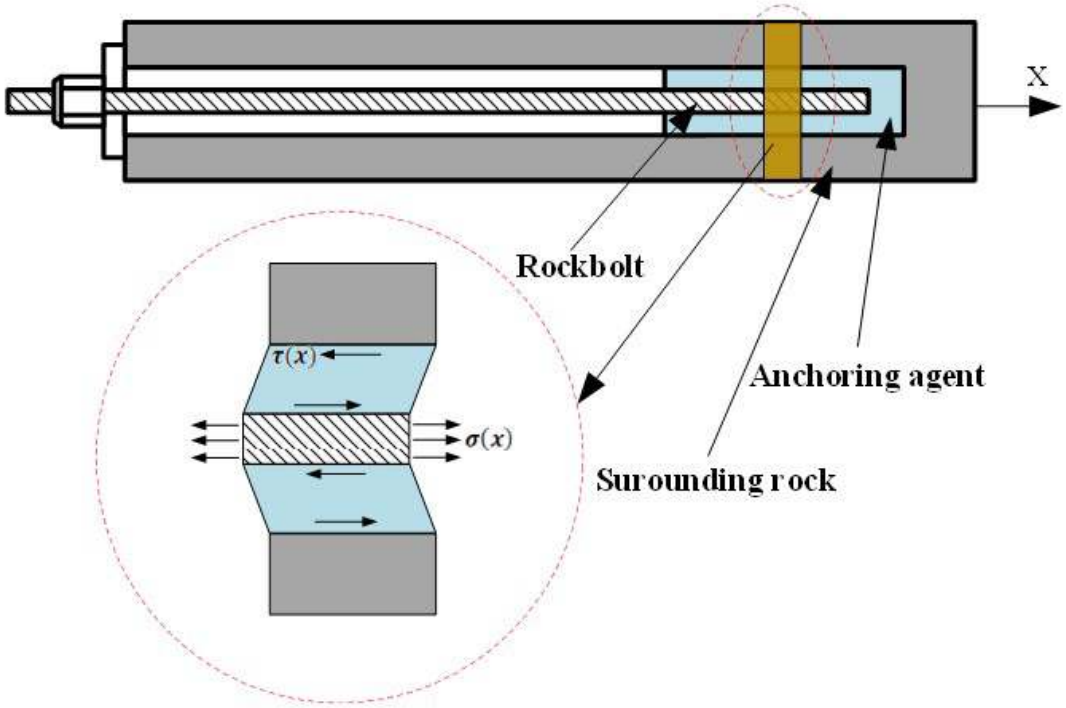

Figure 1 Schematic diagram of the end-anchored rockbolt.

To evaluate the impact performance of the rockbolts, scholars from different countries have conducted research on various testing methods, primarily including laboratory experiments and numerical simulations (Masoudi and Sharifzadeh 2018). In terms of laboratory tests, according to the design principle, the widely used test facilities can be divided into three categories. One is the drop weight free fall impact test method based on the principle of energy transfer, the schematic diagram of the test device is shown in Figure 2(a), the representative facility is CANMET-MMSL drop testing machine (Vallejos et al. 2020; Sharifzadeh et al. 2020a). The second is a test method based on the principle of momentum transfer, which transfers the momentum of the hammer to the rockbolt. At present, the representative facility is a test facility developed by the University of Mining and Technology of Western Australia (WASM). The third is the Hopkinson bar impact test based on the principle of stress wave transmission. This testing machine has a wide range of applications in studying the material response under dynamic loading conditions and the material properties under high speed impact loads (Gama et al. 2004). In addition to these, other facilities such as the comprehensive test platform for static-dynamic rockbolt mechanical properties developed by Kang et al. (2020) is also in operation. Charette and Plouffe (2008) evaluated the impact resistance of a new type of rockbolt called Roofex using the CANMET-MMSL drop

weight impact testing machine. They applied up to 27 kJ of impact energy on the Roofex rockbolt, which was fully absorbed by the rockbolt. Sharifzadeh et al. (2020b) conducted numerous experiments and proposed a simplified model equivalent to the dynamic response curve from the perspective of energy absorption. They found that the average impact load remained approximately constant during the dynamic testing process. Li and Doucet (2012) used the CANMET-MMSL testing machine to evaluate a newly invented yielding rockbolt called the D-bolt. The testing confirmed the excellent energy absorption characteristics and impact resistance of the D-bolt. Varden et al. (2008) improved the Garford rockbolt based on the results of rockbolt impact tests. It is specifically designed to sustain a consistent deformation when subjected to impacts by employing a yielding mechanism. Once the designated energy absorption capacity is nearly exhausted, the deformation of the rockbolt is securely locked in place through a specialized end braking mechanism. In terms of numerical simulation research, Nguyen et al. (2019) simulated the drop weight impact test of rockbolt using explicit finite element method. The simulation results showed good agreement with laboratory test results, providing a basis for studying the dynamic characteristics of the rockbolt using finite element method. Zhao et al. (2021a) conducted numerical simulations of the end-anchored rockbolt under drop weight impact using Abaqus software. They revealed the stress distribution characteristics and evolution laws of end-anchored rockbolts under dynamic loads. Marambio et al. (2018) simulated indoor tests using a numerical simulation method based on finite difference method. They compared and adjusted the numerical model with previous indoor dynamic rockbolt tests, and predicted the performance of threaded steel rockbolts under dynamic load tests. John and Dillen (1983) developed a new constitutive model of rockbolt by using computer programming language, which can better characterize the mechanical properties of fully grouted rockbolt in roadway under the influence of dynamic load. Lou et al. (2023) conducted split tube drop tests with different impact energies to better understand the dynamic performance of MP1 rockbolt under various earthquake event magnitudes and mitigate rockburst damage during underground excavation during seismic activity.

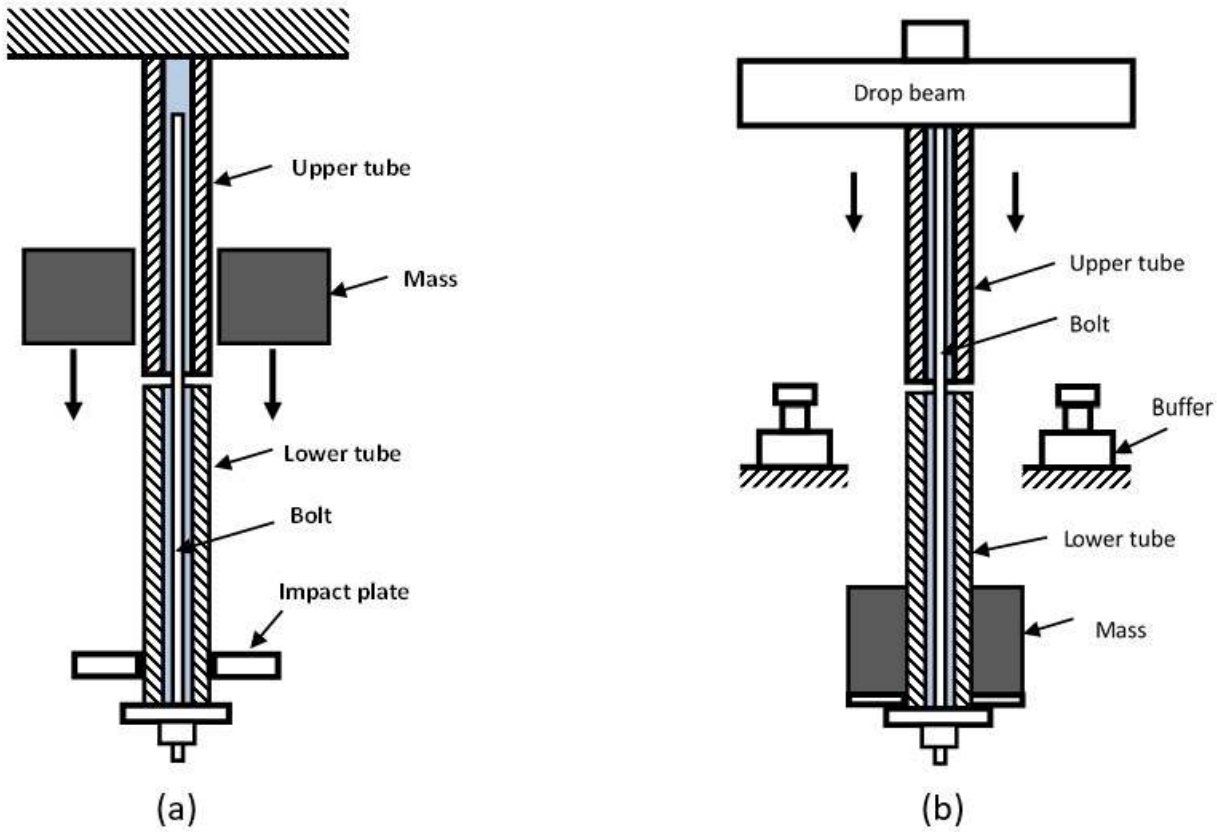

Figure 2 Common dynamic testing machines for rockbolt: (a) CANMET-MMSL testing machine; (b) WASM testing machine (Li 2017).

Scholars have done a lot of research on the force, deformation and energy absorption of rockbolts under dynamic loading. Previous studies focused on the influence of surrounding rock strength on the rockbolt reinforcement mechanism, often ignoring the influence of surrounding rock stiffness. In the field engineering, due to the mining disturbance and different rock lithology, it makes the radial stiffness of surrounding rock inevitably have variability. The

study of the effect of radial stiffness on the dynamic characteristics of end-anchored rockbolt can help to further explain the reinforcement mechanism under dynamic loading. In this paper, the dynamic mechanical response of end-anchored rockbolt under different rock radial stiffnesses is investigated by numerical simulation, and the changes of anchor impact force and bolt bar deformation are analyzed. Then, the effect of radial stiffness on the energy-absorbing characteristics of end-anchored rockbolt was evaluated based on three characteristic quantities, including the value of absorbed impact energy, specific plastic energy (SPE), and energy absorption rate (EAR). Finally, the effects of impact energy and rock radial stiffness on the breaking mode of anchor rods were investigated.

2 THICKNESS OF STEEL TUBE WITH DIFFERENT RADIAL STIFFNESS

2.1 Theory of equivalent radial stiffness

Due to limitations in conditions, steel tubes with a certain wall thickness are often used to simulate surrounding rock mass in indoor experiments and numerical simulations. Kang et al. (2014) used steel tube to simulate rock mass in their study on the axial stress distribution of rockbolts under tensile conditions and the influence of various variables on anchoring performance. Zhao et al. (2020) used steel tubes to simulate surrounding rock in rockbolt impact tests to investigate the effect of damping ratio on the energy-absorbing characteristics of their newly developed rockbolt. Li et al. (2021) used steel tubes to simulate rockbolt boreholes in order to study the differences in rockbolt impact testing machines among four laboratories in different countries. They conducted a series of impact tests on the same rockbolts using direct impact method and found significant equipment-dependent deviations in the results. Most scholars use steel tube to simulate surrounding rock in drop weight impact test of the rockbolt. In order to obtain more reliable test results, the radial stiffness of steel tube must be matched with the radial stiffness of borehole in surrounding rock. Under the condition of a certain inner diameter of the steel tube, the thickness of the steel tube is directly related to the radial stiffness of the surrounding rock. The schematic diagram of the calculation model is shown in Figure 3.

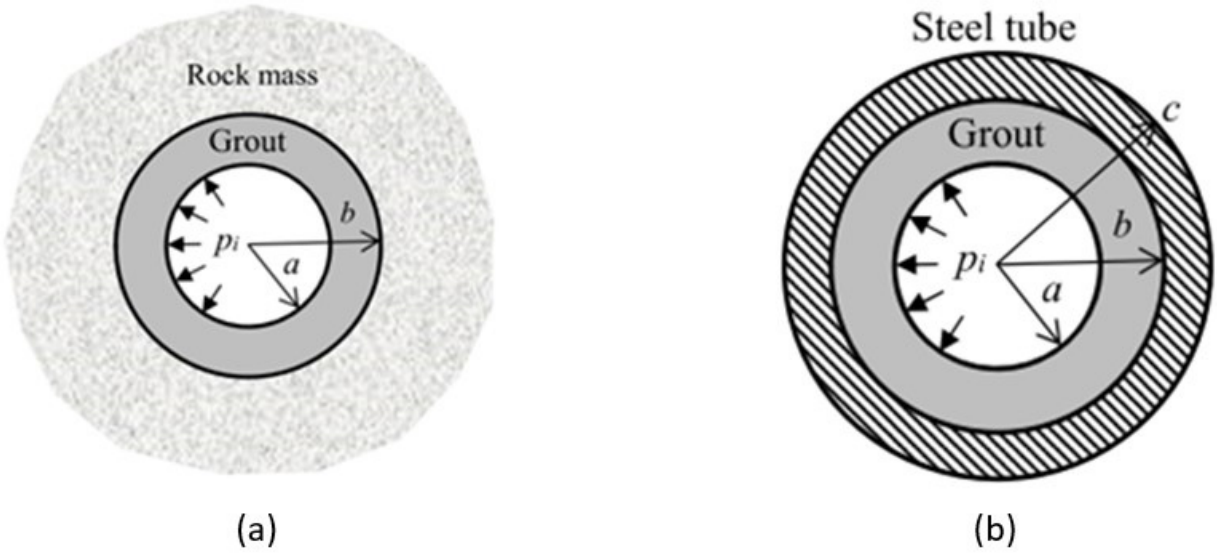

Figure 3 Calculation model of surrounding rock of grouting rockbolt (Zhao et al. 2021b): (a) Calculation model of surrounding rock of grouting rockbolt; (b) Calculation model of steel tube in laboratory.

Zhao et al. (2021b) proposed a calculation formula that determines the relationship between the thickness of steel tube and radial stiffness of the surrounding rock. By separately calculating the radial stiffness of the surrounding rock and the radial stiffness of the steel tube, the two can be equated to determine the required thickness of the steel tube for different levels of radial stiffness of surrounding rock. The expression for calculating the thickness is as follows:

$$K_{\mathrm{r}} = \frac{E_{\mathrm{r}}}{b(1-v_{\mathrm{r}})} \tag{1}$$

$$K_s = \frac{E_s(c^2 - b^2)}{b^3(1 - v_s) + bc^2(1 + v_s)} \tag{2}$$

$$t = b\left(\sqrt{\frac{(1+v_r)E_s/E_r - v_s + 1}{(1+v_r)E_s/E_r - v_s - 1}} - 1\right) \tag{3}$$

In the above formulas (1) to (3), t represents the thickness of the steel tube, b and c are the inner radius and outer radius of the steel tube, respectively. E_s and v_s are the Young's modulus and Poisson's ratio of the steel tube, respectively. E_r and v_r are the Young's modulus and Poisson's ratio of the surrounding rock, respectively. K_s and K_r are the radial stiffness of the steel tube and the surrounding rock, respectively.

2.2 Calculation of thickness of steel tube wall

In order to study the influence of the radial stiffness of the surrounding rock on the dynamic characteristics of the end-anchored rockbolt, based on the relationship between the thickness of the steel tube and the radial stiffness of the surrounding rock in the above theory, the thickness of the steel tube with a diameter of 35 mm (Li and Doucet 2012) corresponding to different radial stiffness of the surrounding rock is obtained. See Table 1 for details.

Table 1 Correspondence between steel tube wall thickness and radial stiffness..

Group number	Young's modulus of rock (GPa)	Poisson's ratio of rock	Young's modulus of steel tube (GPa)	Poisson's ratio of steel tube	Thickness of steel tube (mm)	Radial stiffness (GPa·mm^{-1})
1	7.19	0.25	206	0.3	0.5	0.33
2	20.62	0.25	206	0.3	1.5	0.94
3	26.89	0.25	206	0.3	2	1.23
4	32.87	0.25	206	0.3	2.5	1.50
5	38.59	0.25	206	0.3	3.0	1.76
6	44.05	0.25	206	0.3	3.5	2.01
7	49.27	0.25	206	0.3	4.0	2.25
8	54.26	0.25	206	0.3	4.5	2.48
9	63.58	0.25	206	0.3	5.5	2.91
10	72.12	0.25	206	0.3	6.5	3.29
11	79.93	0.25	206	0.3	7.5	3.65
12	93.68	0.25	206	0.3	9.5	4.28

3 MATERIALS AND METHODS

3.1 Finite element model

This study is based on the drop weight impact test method for the end-anchored rockbolt. A numerical model of the dynamic impact of rockbolt is established using the Abaqus software. The model consists of six parts: rockbolt, resin, steel tube, drop weight, tray, and nut, as shown in Figure 4. The length of the end-anchored rockbolt in the test is 2.0 m, with the end portion anchored. A nut and a circular tray are installed at the free end of the rockbolt, and the rockbolt is installed within a hollow steel tube using resin. In the actual finite element model, the end of the steel tube at the end of the rockbolt is set as a fixed constraint, the drop weight is applied with an initial velocity and gravity acceleration, and the nut and the tray are respectively set as binding constraints with the rockbolt. The detailed dimensions of each component in the numerical model can be found in Table 2. The drop weight mainly serves as the energy source for impact. These components of the model are divided into mesh, with the element type set as C3D8R. The model contains approximately 18,000 meshes.

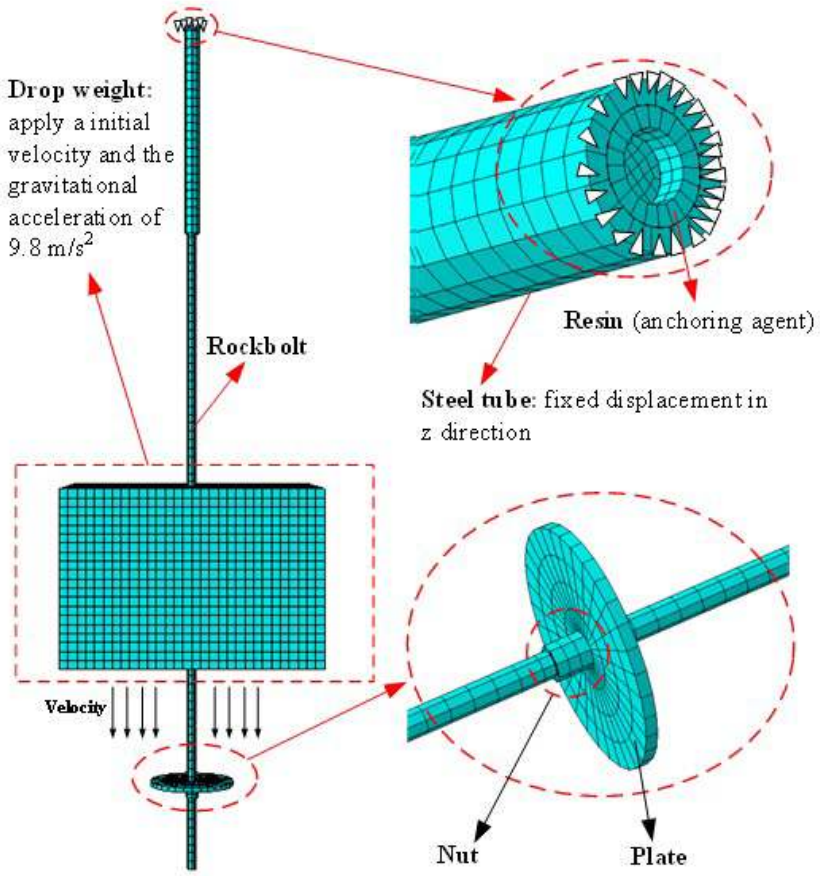

Figure 4 Numerical model of dynamic impact for the rockbolt.

Table 2 Detailed dimensions of each component of numerical model.

Part Name	Length (mm)	External diameter (mm)	Inner diameter (mm)
Rockbolt	2000	22	-
Resin	500	35	22
Steel tube	500	-	35
Plate	10	200	22
Nut	30	30	22

3.2 Model parameter

The static yield criterion for rockbolt adopts the classic Mises yield criterion. Studies have found that the mechanical properties of steel change under dynamic loading conditions. Specifically, under dynamic loading, the tensile strength and yield strength of the steel increase by a certain coefficient. The dynamic parameters of the steel can be estimated based on the static parameters by scaling them with a dynamic increase coefficient (DIF). Malvar and Crawford (1998) recommend that the DIF is applicable to steels with a static yield strength ranging from 290 MPa to 710 MPa and a strain rate between 10^{-4} s^{-1} and 225 s^{-1}. To accurately describe the mechanical behavior of end-anchored rockbolt under impact loads in numerical simulations, the end-anchored rockbolt is modeled using the built-in metal ductile damage model in the Abaqus software.

$$DIF = \left(\frac{\dot{\varepsilon}}{10^{-4}}\right)^{\alpha} \tag{4}$$

$$\alpha_{f_y} = 0.074 - 0.040\,\frac{f_y}{414} \tag{5}$$

$$\alpha_{f_u} = 0.019 - 0.009\frac{f_u}{414} \tag{6}$$

where $\dot{\varepsilon}$ is the strain rate, f_y is the static yield strength of steel (unit MPa); α_{f_y} and α_{f_u} are the static yield strength and static tensile strength coefficient of steel, respectively.

The resin is modeled using an ideal elastic-plastic constitutive model, while the steel tube is modeled using an elastic constitutive model. The drop weight, nut, and tray are simulated as rigid body. In terms of contact settings, the interface constitutive model used is the adhesive property and Coulomb friction built-in in Abaqus, and a bonding force of 20 MPa is set between the rockbolt and the resin to simulate the bonding effect. The bonding force between the resin and the steel tube is set to 30 MPa (Si et al. 2022). The other components are set as bond contact with the end-anchored rockbolt. The rockbolt material is made of BHRB500 steel, which is widely used in China. The mechanical parameters of the rockbolt material are listed in Table 3, and the mechanical parameters (Zhao et al. 2021a) of other components of the numerical model are listed in Table 4.

Table 3 Numerical model parameters of end-anchored rockbolt

Bolt diameter (mm)	Density (kg·m^{-3})	Young's modulus (GPa)	Poisson's ratio	Yield strength (MPa)	Tensile strength (MPa)
22	7800	210	0.28	500	610

Table 4 Numerical model parameters of other components

Part Name	Constitutive model	Density (kg·m^{-3})	Young's modulus (GPa)	Poisson's ratio
Plate	Elastic model	7800	200	0.28
Steel tube	Elastic model	7850	200	0.25
nut	Elastic model	7800	200	0.25
Resin	Ideal Elastic-Plastic	2000	25	0.32
Drop weight	Rigid body	Assigning a mass of 671Kg.		

3.3 Simulation plan

In the following simulation scheme, according to the matching relationship between the radial stiffness of surrounding rock and the wall thickness of steel tube in Table 1, the numerical models of different radial stiffness are established respectively. In each numerical simulation, the energy of 10 kJ produced by the free falling of drop weight acts on the end-anchored rockbolt, and the impact energy is mainly absorbed by the rockbolt, resin and anchorage interface. This paper will carry out simulation research from the following three aspects.

(1) Keeping the impact velocity and the mass of the drop weight unchanged, the fixed impact energy is 10 kJ. By adjusting the wall thickness of the steel tube, the influence of the radial stiffness of the surrounding rock on the force and displacement of the end-anchored rockbolt is studied under the condition that the radial stiffness of the surrounding rock is 1.50, 2.01, 2.25, 2.91, 3.29GPa/mm, respectively. The specific simulation scheme is shown in Table 5.

Table 5 Simulation scheme under different radial stiffness conditions.

Number	Initial velocity (m·s^{-1})	Impact energy (kJ)	Thickness of steel tube (mm)	Radial stiffness (GPa·mm^{-1})
1	5.46	10	2.5	1.50
2	5.46	10	3.5	2.01
3	5.46	10	4.0	2.25
4	5.46	10	5.5	2.91
5	5.46	10	6.5	3.29

(2) Keeping the impact velocity and the mass of the drop weight unchanged, the fixed impact energy is 10 kJ. When the radial stiffness of surrounding rock is 1.50, 2.01, 2.25, 2.91, 3.29GPa/mm respectively, the influence of radial stiffness on the energy absorption characteristic of end-anchored rockbolt is studied. The simulation scheme is shown in Table 5.

(3) According to the kinetic energy formula $E_k = 0.5mv^2$ and the matching relationship between the wall thickness of the steel tube and the radial stiffness of the surrounding rock, the fracture position of the end-anchored rockbolt with the impact energy range of 40 to 90kJ and the radial stiffness of the surrounding rock range of 1.50 to 3.82GPa/mm is studied respectively. The simulation scheme is shown in Table 6.

Table 6 Simulation scheme under different radial stiffness and impact energy conditions

Number	Impact energy (kJ)	Thickness of steel tube (mm)	Radial stiffness (GPa·mm^{-1})
1	40	2.5~8.0	1.50~3.82
2	50	2.5~8.0	1.50~3.82
3	60	2.5~8.0	1.50~3.82
4	70	2.5~8.0	1.50~3.82
5	80	2.5~8.0	1.50~3.82
6	90	2.5~8.0	1.50~3.82

4 RESULTS

4.1 Dynamic response of the end-anchored rockbolt

The radial stiffness of surrounding rock is often closely related to the stability of anchorage system composed of rockbolt, surrounding rock and anchorage agent. When a rockbolt is subjected to dynamic loads, the dynamic response of the rockbolt can vary under different surrounding rock radial stiffness conditions. Therefore, it is necessary to investigate the influence of surrounding rock radial stiffness on the dynamic response of rockbolt in order to provide more instructive support or monitoring and warning solutions.

Under the action of impact, the curve of impact load with time is shown in Figure 5(a). With the increase of radial stiffness of surrounding rock, the fluctuation of impact force time history curve decreases gradually, and the load transfer is more stable. The time of the whole impact process is slightly different. It can be seen that the increase of radial stiffness can make the anchorage system more stable. When the stiffness of surrounding rock is small, the stress fluctuation of anchorage system is large. The time-history curve of the elongation of the rockbolt during the impact process is shown in Figure 5(b). With the increase of the radial stiffness of the surrounding rock, the maximum value of the elongation gradually increases, and the final elongation gradually decreases. This means that when the radial stiffness of the surrounding rock is smaller, the elastic deformation generated by the anchorage system is greater. When the radial stiffness of the surrounding rock is greater than 2.25GPa/mm, the maximum elongation and the final elongation reach a stable value, which is no longer affected by the radial stiffness of the surrounding rock.

The corresponding curve between impact force and elongation is shown in Figure 6. In the initial stage of impact, it is evident that the slope of the load-displacement curve varies with the radial stiffness of surrounding rocks. As the radial stiffness of the surrounding rock increases, the initial slope shows a generally upward trend. Considering the control equation of dynamic problems, it not only takes into account the system stiffness but also considers damping and inertia terms, where damping and inertia terms often dominate. However, at the initial moment of the impact, the velocity and acceleration are small, and the stiffness of the anchorage system contributes more to the initial slope. The initial slope can be considered as the initial stiffness. In the midterm stage of the impact, the end-anchored rockbolt continues to elongate and enters the plastic flow stage, where the variation of impact force becomes relatively stable compared to the initial stage. In the final stage affected by the impact, the stored elastic potential energy from the elongation of the end-anchored rockbolt gradually becomes dominant. The rockbolt body starts to rebound, and the impact force gradually decreases.

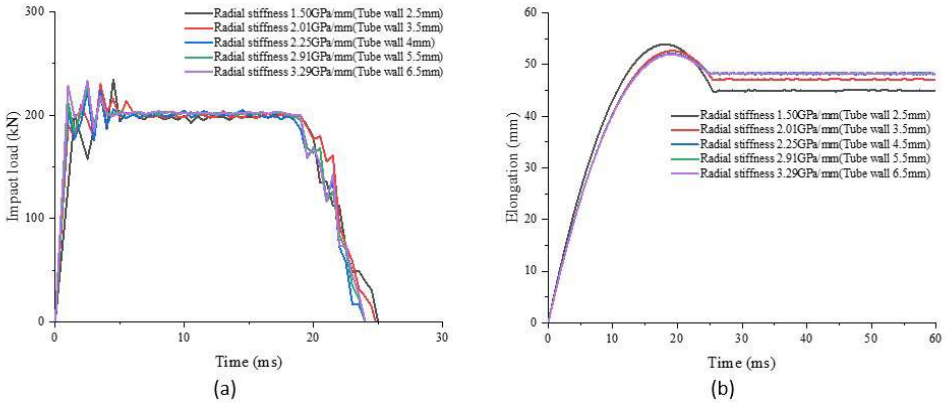

Figure 5 Curves of impact load and elongation of rockbolt under different radial stiffnesses: (a) Impact load time history curve of rockbolt; (b) Elongation time history curve of rockbolt.

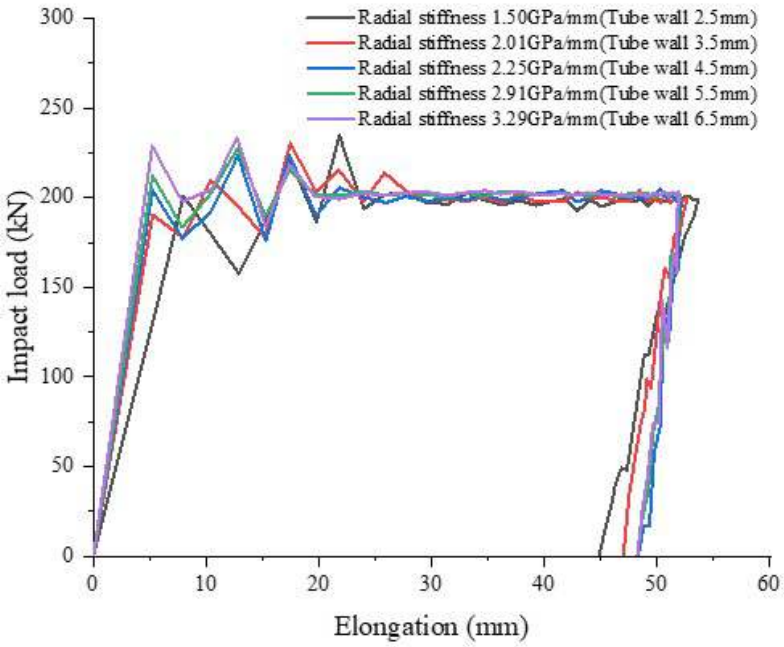

Figure 6 Impact force vs elongation curves of rockbolt under different radial stiffness.

4.2 Energy absorption characteristics of the end-anchored rockbolt

To further investigate the influence of the radial stiffness of surrounding rock on the energy absorption characteristics of end-anchored rockbolt, Figure 7 (a), 8 (a), 9 (a), and 10 (a) present the energy absorption curves of the end-anchored rockbolt under four different radial stiffnesses of surrounding rock, as obtained through numerical simulations. Li et al. (2021) proposed the use of specific plastic energy (SPE) as the measure of average impact load. As shown in Figure 7 (a), the shaded region beneath the curve represents the energy dissipation due to plastic deformations of the end-anchored rockbolt, referred to as Plastic Dissipation Energy (PE). The ratio of Plastic Dissipation Energy to the final displacement (D) can be regarded as the Average Impact Load (AIL), which also represents the amount of energy absorbed by the rockbolt per unit plastic displacement, commonly known as specific plastic energy (SPE). For radial stiffness values of 1.50GPa/mm, 2.25GPa/mm, 2.91GPa/mm, and 3.29GPa/mm, the corresponding SPE values are 197.3kN, 198.1kN, 200.6kN, and 202.5kN, respectively. This illustrates that with an increase in radial stiffness, the Specific Plastic Energy (SPE) also increases.

$$AIL = SPE = \frac{PE}{D} \tag{7}$$

As shown in Figure 7 (b), 8 (b), 9 (b), and 10 (b), the integrated curves of impact load against elongation and their fitting lines are presented. The integrated curves mainly reflect the correspondence between energy absorption and elongation during the impact process. The slope of the fitting line of the integrated curve is a measure of the average energy absorption per unit length deformation throughout the entire impact process. It should be noted that the analysis here includes the rebound stage of the end-anchored rockbolt, which is the process of energy release or recovery. Therefore, the integrated curve comprehensively reflects the entire process of energy absorption and release of the end-anchored rockbolt. The slope of the curve is referred to as energy absorption rate (EAR), which represents the total energy absorbed per unit length. The energy absorption rate (EAR) is also a parameter widely used to characterize the energy absorption characteristics of the rockbolt. The mechanical meaning of the energy absorption rate (EAR) is similar to that of the SPE, and both units are kN. Both parameters can represent the average impact load to some extent. The main difference is that EAR takes into account both the plastic and elastic energy, representing the statistical average of the average elastic and plastic energy per unit length deformation, while SPE represents the average plastic energy per unit length deformation. When the radial stiffness of surrounding rock is 0.94GPa/mm, 2.01GPa/mm, 2.25GPa/mm, and 3.65GPa/mm, the slopes of the fitting lines for the relationship between the energy absorption rate and elongation are 197.6kN, 200.0kN, 202.0kN, and 203.0kN, respectively. This indicates that with an increase in radial stiffness of surrounding rock, the energy absorption rate also increases.

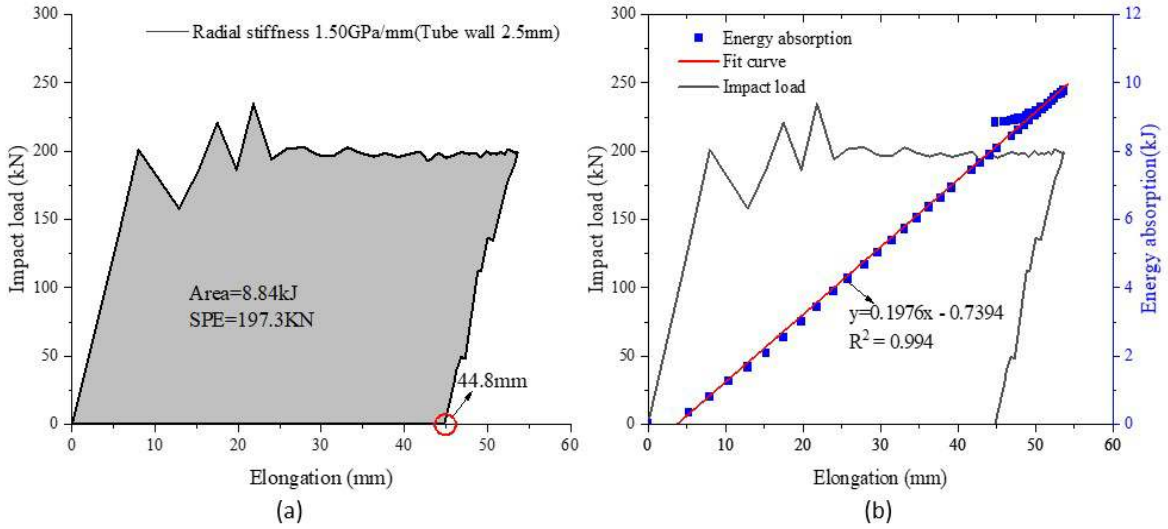

Figure 7 Variation of cumulative energy absorption with the shank deformation: (**a**) Energy absorption(1.50GPa/mm); (**b**) Energy absorption rate(1.50GPa/mm).

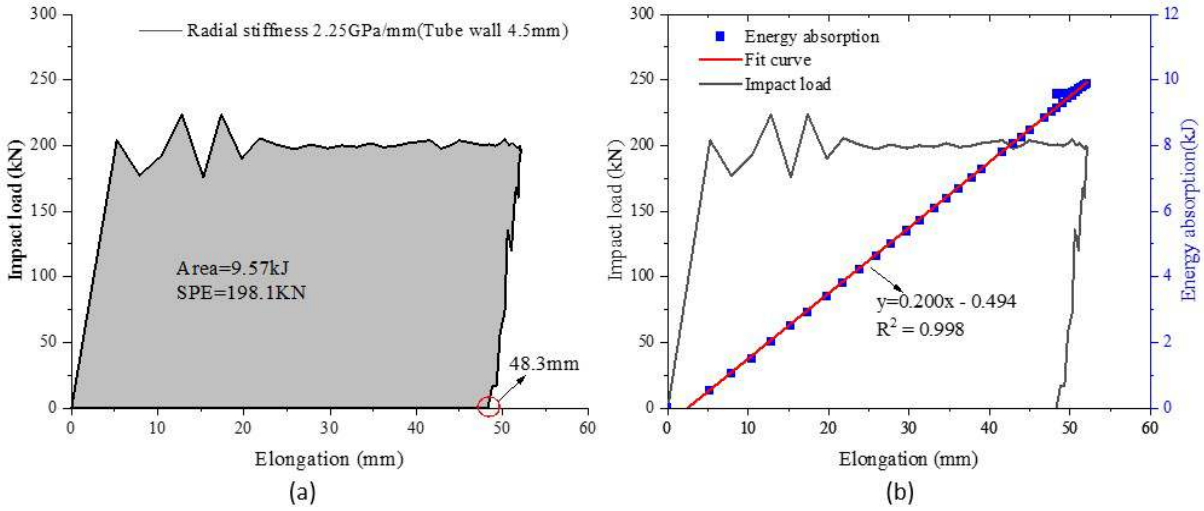

Figure 8 Variation of cumulative energy absorption with the shank deformation: (**a**) Energy absorption(2.25GPa/mm); (**b**) Energy absorption rate(2.25GPa/mm).

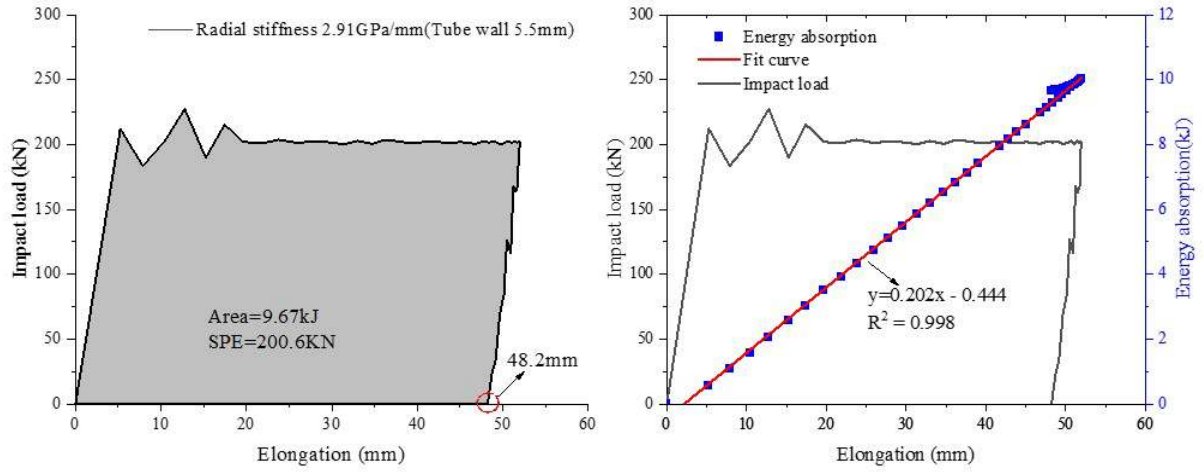

Figure 9 Variation of cumulative energy absorption with the rockbolt deformation: (a) Energy absorption(2.91GPa/mm); (b) Energy absorption rate(2.91GPa/mm).

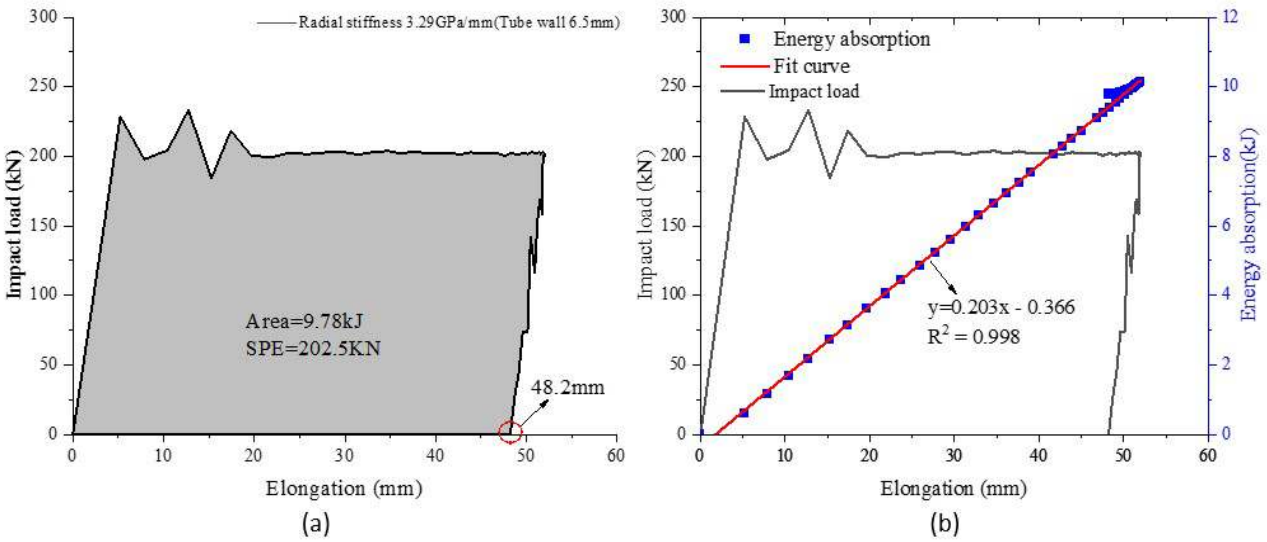

Figure 10 Variation of cumulative energy absorption with the rockbolt deformation: (a) Energy absorption(3.29GPa/mm); (b) Energy absorption rate(3.29GPa/mm).

With the increase in the radial stiffness of the surrounding rock, the energy absorption of the end-anchored rockbolt can be roughly divided into three cases, as shown in Figure 11. When the rock stiffness is less than or equal to 0.94GPa/mm, the rockbolt completely slips off, and the energy is mainly absorbed by the failure and friction of the anchoring agent and anchoring interface. When the radial stiffness of surrounding rock is greater than 0.94GPa/mm and less than 1.23GPa/mm, partial slippage occurs in the rockbolt, and the energy absorption is mainly due to the elongation of the rockbolt itself, while a small amount of energy is absorbed by the failure and friction of the anchoring agent and anchoring interface. Once slippage occurs, the displacement of the elongation monitoring point begins to be dominated by rigid body displacement, which does not conform to the calculation principle of specific plastic energy (SPE) and energy absorption rate (EAR). The energy absorption amount can still be used to describe the energy absorption characteristics of the rockbolt. Therefore, the radial stiffness of the surrounding rock is less than 1.23GPa / mm, which belongs to a class of cases. When the rock radial stiffness is greater than 1.23GPa/mm and less than 2.91GPa/mm, the radial stiffness of the surrounding rock significantly influences the energy absorption characteristics of the anchorage system, and both SPE and EAR are sensitive to changes in radial stiffness. When the radial stiffness exceeds 2.91GPa/mm, the curves of these two energy absorption parameters become closer, indicating a stable stage where changes in radial stiffness have less influence.

In order to further study the relationship between the radial stiffness and the energy absorption characteristics of rockbolt. as shown in Figure 11 (a), it is a nonlinear fitting curve of the relationship between the radial stiffness of the surrounding rock and the energy absorption. The fitting formula is shown in (8). With the increase of the radial stiffness of the surrounding rock, the energy absorption also increases according to the negative exponential law. Finally, when the stiffness of the surrounding rock is large, it converges to a certain value. Both Specific Plasticity Energy (SPE) and Energy Absorption Rate (EAR) are important indicators for characterizing the energy absorption characteristics of rockbolts. They both represent the energy absorption per unit length of rockbolt deformation, and can also reflect the average impact force. Figure 11(b) shows the nonlinear fitting curves of SPE and EAR with respect to the radial stiffness respectively, and the expressions of the fitting curves for EAR and SPE are given in Equations (9) and (10), respectively, where S represents the radial stiffness of the surrounding rock. The coefficients of determination (R^2) for these parameters are 0.92 and 0.96, indicating that they can effectively describe the relationship between SPE, EAR, and rock radial stiffness in underground engineering. Their determination coefficients R^2 are 0.99, 0.91 and 0.94 respectively. Therefore, these fitting formulas can better describe the relationship between the energy absorption characteristics of the rockbolt and the radial stiffness of the surrounding rock.

$$E = 9.8 - 36.3e^{-2.4S} \tag{8}$$

$$SPE = 202.6 - 439.4e^{-2.6S} \tag{9}$$

$$EAR = 203.2 - 238.4e^{-2.2S} \tag{10}$$

It can be seen from Figure 11(b) and the fitting curve formulas (8) and (9) that when the radial stiffness of the surrounding rock increases, the specific plastic energy (SPE) and energy absorption rate (EAR) also increase gradually. When the radial stiffness of the surrounding rock tends to infinity, they reach the maximum values of 202.6kN and 203.2kN, respectively. The lower limit of the fitting formula is the corresponding radial stiffness of the surrounding rock When the rockbolt anchorage interface produces slip failure.

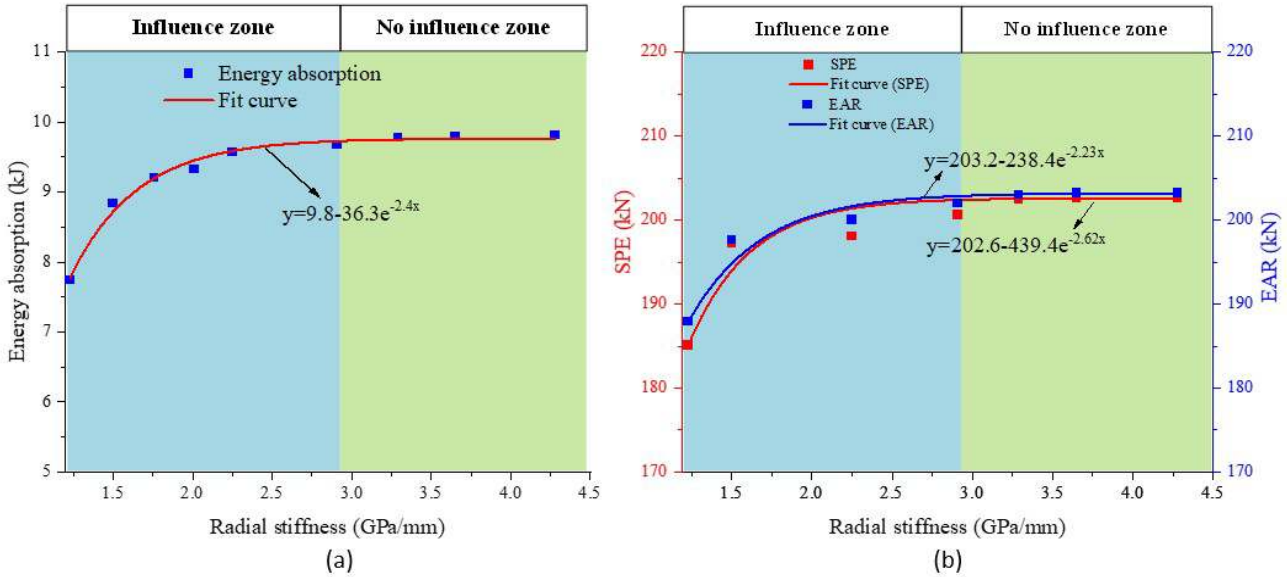

Figure 11 Relationship between radial stiffness of surrounding rock and energy absorption: (a) Energy absorption; (b) Characteristic quantitys of energy absorption.

4.3 Fracture position of rockbolt under impact load

In cases where the surrounding rock has very weak rock stiffness or the interface bonding strength is low, debonding or rock mass failure often occurs near the anchorage interface. When debonding occurs, the majority of the impact energy cannot be absorbed by the rockbolt, and the energy absorption capacity of the rockbolt in the anchorage system cannot be fully utilized. Therefore, it is necessary to further study the fracture position of the rockbolt.

Fracture failure often occurs in localized areas with significant plastic deformation, while other regions experience smaller deformations. This means that the energy generated by impact is primarily absorbed through local elongation deformation of the end-anchored rockbolt. The material in this localized region will experience early damage, and once the damage reaches a certain extent, the material will fail to carry load and fracture occurs. Therefore, under certain conditions, the location of fracture failure is not random but confined to a specific local range. If this range, where failure is prone to occur, can be determined, local reinforcement or installation of special energy-absorbing structures within this range can further enhance the overall energy absorption characteristics of the end-anchored rockbolt. As shown in Figure 12 (a), under the condition that the radial stiffness of the surrounding rock is 3.29 GPa / mm and the impact energy is 40 kJ, the plastic strain cloud diagram of the free section of the end-anchored rockbolt at different time points is shown. As the rockbolt body continues to elongate to absorb energy, significant local plastic deformation gradually occurs. Under the current conditions of radial stiffness of surrounding rock and impact energy, the occurrence of localized large deformations is located near the anchoring interface until the energy absorption limit is reached, leading to fracture. Figure 12 (b) shows the distribution of plastic strain at different locations of the free section of the end-anchored rockbolt during the impact process. Two obvious extreme points of plastic strain can be observed in the figure, located near the tray and the anchoring interface, respectively. The position range centered around these two extreme points represents the localized large deformation zone. The extreme point near the tray is caused by direct impact, while the peak point near the anchoring interface is due to complex stress wave interactions, such as reflection waves, transmission waves, and various interface waves, after the stress wave reaches the anchoring interface. The coupling of these stress waves generates new stress waves, resulting in a highly complex stress field at the anchoring interface and causing an increase in local stress.

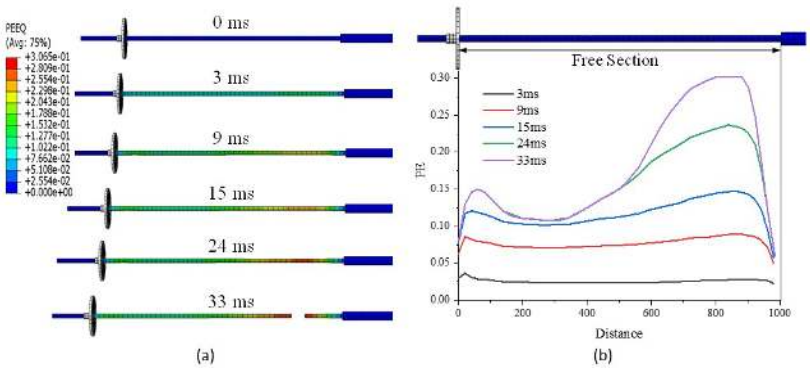

Figure 12 Plastic strain in the rockbolt: (a) Plastic strain cloud map; (b) Plastic strain along the length of free section.

The local deformation generated under impact is the main cause of eventual failure and fracture. Determining the location range of local deformation is of great significance for the reinforcement of steel rockbolts and the development of new rockbolts. Among the external factors affecting the dynamic characteristics of the rockbolt, the impact energy and surrounding rock conditions are the main ones, as opposed to rockbolt type and anchoring agent type. When the end-anchored rockbolt is subjected to a higher impact, it can produce local large deformation, which eventually leads to the fracture of the end-anchored rockbolt. When the radial stiffness of the surrounding rock is greater than 1.50 GPa / mm and the energy is very high, about 100 kJ, the tray, which is the first to be directly affected by the impact, is first destroyed. When the radial stiffness of the surrounding rock is greater than 1.50 GPa / mm and the impact energy is in the range of 40 kJ to 90 kJ, the end-anchored rockbolt breaks near the anchorage end, as shown in Figure.13 (a). As shown in Figure 13 (b), the change of the distance between the fracture position of end-anchored rockbolt and the anchorage end under different radial stiffnesses of the surrounding rock can be divided into three intervals according to the different influence of radial stiffness of the surrounding rock on the results. When the radial stiffness of the surrounding rock is less than or equal to 1.23 GPa / mm, the anchorage interface slip failure occurs, which is not the research content of this paper. When the radial stiffness of the surrounding rock is greater than 2.01 GPa / mm and less than 2.91 GPa / mm, the radial stiffness of the surrounding rock has a significant effect on the location of the fracture of the rockbolt body, and the two show a positive correlation. Under other radial stiffness of the surrounding rock ranges, the radial stiffness of the surrounding rock has almost no effect on the fracture position of the rockbolt body.

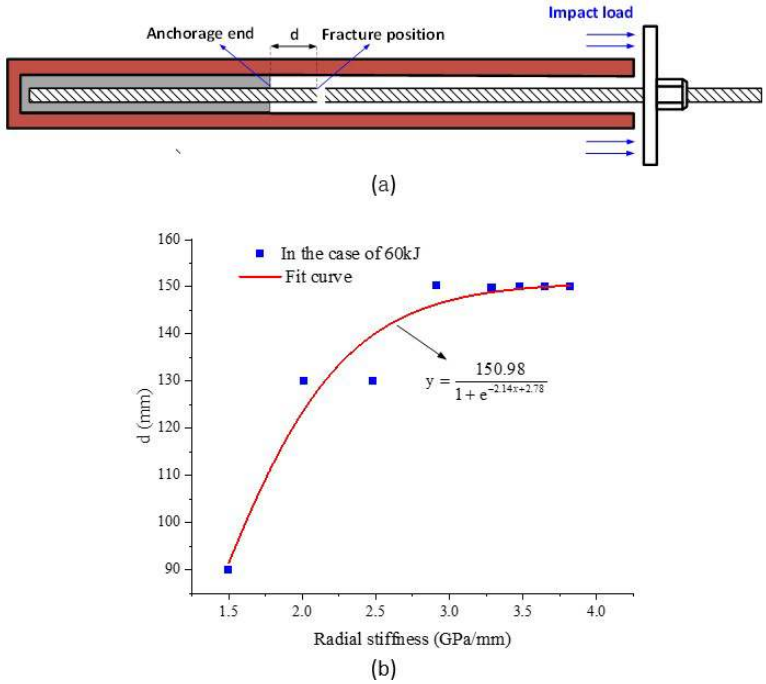

Figure 13 Influence of radial stiffness of surrounding rock on fracture location: (a) Fracture diagram of end-anchored rockbolt; (b) Distance between the fracture position of the rockbolt and the anchorage end under different radial stiffnes.

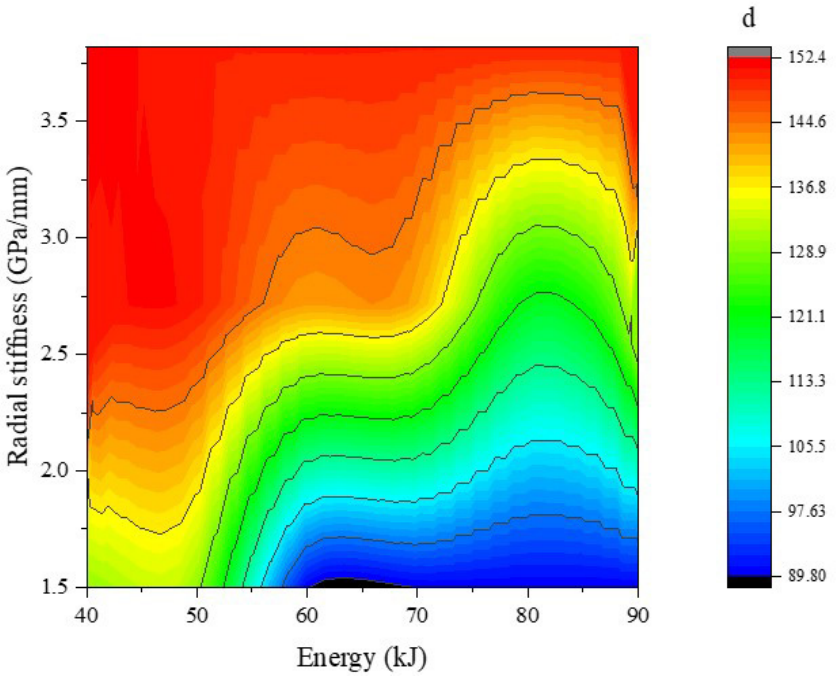

Figure 14 Contour plot of fracture position values.

In order to further reveal the influence of radial stiffness of surrounding rock and impact energy on the fracture position of the rockbolt, taking the radial stiffness and impact energy as independent variables, and the distance between the fracture position of the rockbolt and the anchorage end as the dependent variable, the contour of the distance value is drawn as shown in Figure 14. The contour line as a whole shows the characteristics of "left upper high right lower low". When the impact energy is fixed, with the increase of the radial stiffness of the surrounding rock, the distance between the fracture position and the anchorage end shows an increasing trend, which is consistent with the conclusion obtained from the analysis of figure 13 (b). When the radial stiffness is fixed, with the increase of impact energy, the distance between the fracture position and the anchorage end is negatively correlated with the impact energy as a whole. According to the contour map, the maximum value of the distance between the fracture position and the anchorage end is located in the range of radial stiffness of 3.50GPa / mm to 4.28GPa / mm, and the impact energy is 40 kJ to 45 kJ. The size is about 152.4 mm, which is recorded as d_{max}; the minimum value is located in the radial stiffness of 1.50GPa / mm to 1.75GPa / mm, the impact energy is in the range of 60 kJ to 70 kJ, the size is about 89.8 mm, recorded as d_{min}.

5 DISCUSSION

Li et al. (2021) pointed out that the initial stiffness of the anchorage system is mainly affected by the elasticity of the rockbolt sample, but also by the slight plasticity that occurs before the first peak load. It can be found that improving the radial stiffness of the surrounding rock to some extent can also improve the absorption capacity of the end-anchored rockbolt for impact energy. The grouting and shotcrete are common techniques to improve the stiffness of the surrounding rock, and they are very important for the impact resistant support of the roadway. The surrounding rock stiffness and the rockbolt system stiffness should have a matching relationship. Therefore, when the surrounding rock stiffness is determined, the matching of the stiffness of the rockbolt system should be further studied in terms of the composition of the bolt bars and anchoring agents. When the impact energy is 10 kJ and the radial stiffness of the surrounding rock is 3.29 GPa / mm, the energy absorbed per unit of elongation of the end-anchor anchors reaches the upper limit of about 202 kN. At this time, further increase the surrounding rock stiffness will make the surrounding rock accumulate more elastic strain energy, which will trigger the occurrence of rockburst disaster. Therefore, it can be studied from the perspective of energy absorption of the rockbolt material and the components of the anchoring system to further improve the impact resistance capacity and give full play to the energy absorption capacity of the components.

The range of distances between the impact fracture location and the anchored end can be obtained from Figure 14. Considering the influence of the rockbolt length on the results, the ratio of the length of the fracture range L_f to the length of the free section of the anchor L_s is used to represent the fracture mode of the rockbolt, which is called the fracture length ratio, as shown in Fig. 15. Take the length of free section of end-anchored rockbolt in this paper as 1.0m

as an example, the distance of fracture location from anchorage end is 89.8mm ~ 152.4mm, and the fracture length ratio is 6.26%. In engineering practice, we can reinforce the parts that are prone to impact fracture, such as increasing the diameter or replacing it with high-strength metal materials. The determination of the fracture length ratio provides a reference for the design of impact resistant rockbolts.

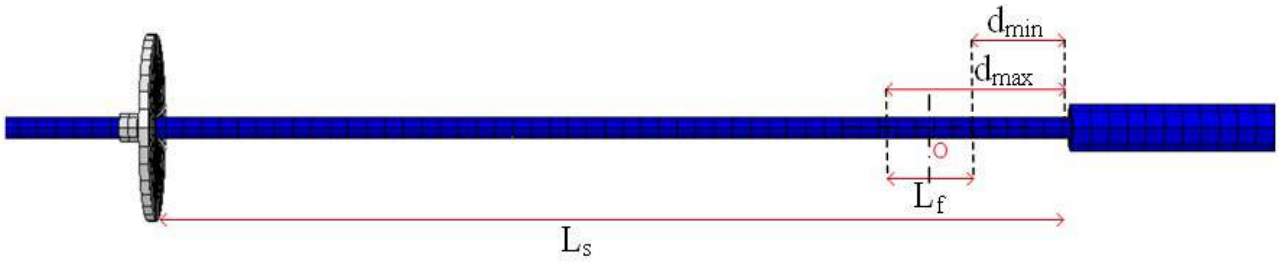

Figure 15 Fracture position diagram.

6 CONCLUSIONS

This paper establishes a numerical model for end-anchored rockbolt under the dynamic impact test, focusing on the dynamic response and energy absorption of rockbolt under different radial stiffness of surrounding rock. The following conclusions can be drawn from the numerical simulation.

(1) As the radial stiffness of the surrounding rock increases, the increment of impact load on the end-anchored rockbolt is relatively small. This indicates that the impact load can be considered constant, while the increment of elongation of the end-anchored rockbolt is more significant. When the radial stiffness varies within a certain range, the initial stiffness of the anchoring system increases with the increase of radial stiffness.

(2) There exists an upper limit to the effect of radial stiffness of the surrounding rock on the energy absorption capacity of the end-anchored rockbolt. When the impact energy is 10 kJ, with the increase of radial stiffness, the effect of radial stiffness on the energy absorption of end-anchored rockbolt can be divided into three zones. They are: when the radial stiffness is less than or equal to 1.23 GPa/mm, rockbolt slipping out occurs at the anchorage interface; when the radial stiffness is greater than 1.23 GPa/mm but less than 2.91 GPa/mm, the energy absorption of the end-anchored rockbolt is significantly affected by the radial stiffness; when the radial stiffness is greater than 2.91 GPa/mm, the radial stiffness has almost no effect on the energy absorption of the end-anchored rockbolt.

(3) The radial stiffness of the surrounding rock and the impact energy are the main factors affecting the dynamic response of end-anchored rockbolt, and they determine the impact fracture range of the rockbolt. The impact fracture length ratio provides a data basis for improving the impact resistance of rockbolt.

ACKNOWLEDGMENTS

This research was funded by National Natural Science Foundation of China (grant number 52104137), Major Program of Shandong Provincial Natural Science Foundation (grant number ZR2019ZD13) and Shandong Provincial Natural Science Foundation (grant number ZR2020QE122).

Author's Contribuitions: Conceptualization, Xingzhong Wu and Yubao Zhang; methodology, Xingzhong Wu and Yubao Zhang; software, Zijian Zhang; validation, Jianye Fu and Pengfei Liu; formal analysis, Zijian Zhang and Longhai Li; investigation, Jianye Fu; Writing - original draft, Xingzhong Wu; Writing - review & editing, Yubao Zhang; supervision, Yubao Zhang and Minglu Xing.

Editor: Marcílio Alves

References

Ren, F.F., Yang, Z., Chen, J., Chen, W. (2010). An analytical analysis of the full-range behaviour of grouted rockbolts based on a tri-linear bond-slip model. Construction and Building Materials 24: 361-370. https://doi.org/10.1016/j.conbuildmat.2009.08.021.

Li, C.C., Kristjansson, G., Høien, A.H. (2016). Critical embedment length and bond strength of fully encapsulated rebar rockbolts. Tunnelling and Underground Space Technology 59: 16-23. https://doi.org/10.1016/j.tust.2016.06.007.

Zhao, T., Xing, M., Guo, W., Wang, C., Wang, B. (2021a). Anchoring effect and energy-absorbing support mechanism of large deformation bolt. Journal of Central South University 28: 572−581. https://doi.org/10.1007/s11771-021-4622-0.

Knox, G., Hadjigeorgiou, J. (2023). Performance of conventional and energy-absorbing self-drilling hollow core rockbolts under controlled laboratory conditions. Rock Mechanics and Rock Engineering 56: 4363-4378. https://doi.org/10.1007/s00603-023-03288-1.

Zhao, C., Zhang, Y., Wu, W., Zhang, Z., Zhao, T. (2021). Numerical study on dynamic performance of end-anchored rockbolt under impact loading. Latin American Journal of Solids and Structures 18: e364. https://doi.org/10.1590/1679-78256458.

Li, C.C. (2010). A new energy-absorbing bolt for rock support in high stress rock masses. International Journal of Rock Mechanics and Mining Sciences 47: 396-404. https://doi.org/10.1016/j.ijrmms.2010.01.005.

He, M., Du, S., Gong, W., Nie, W. (2022). Mechanical characteristics and engineering applications of bolt/cable with negative Poisson's ratio. Mechanics in Engineering 44: 75-87. https://doi.org/10.6052/1000-0879-21-210.

Masoudi, R., Sharifzadeh, M. (2018). Reinforcement selection for deep and high-stress tunnels at preliminary design stages using ground demand and support capacity approach. International Journal of Mining Science and Technology 28: 573-582. https://doi.org/10.1016/j.ijmst.2018.01.004.

Vallejos, J.A., Marambio, E., Burgos, L., Gonzalez, C.V. (2020). Numerical modelling of the dynamic response of threadbar under laboratory-scale conditions. Tunnelling and Underground Space Technology 100: 103263. https://doi.org/10.1016/j.tust.2019.103263.

Sharifzadeh, M., Lou, J., Crompton, B. (2020a). Dynamic performance of energy-absorbing rockbolts based on laboratory test results, Part II: Role of inherent features on dynamic performance of rockbolts. Tunnelling and Underground Space Technology 105: 103555. https://doi.org/10.1016/j.tust.2020.103555.

Gama, B.A., Lopatnikov, S.L., Gillespie, J.W., Jr. (2004). Hopkinson bar experimental technique: A critical review. Applied Mechanics Reviews 57: 223-250. https://doi.org/10.1115/1.1704626.

Kang, H., Yang, J., Gao, F., Li, J. (2020). Experimental study on the mechanical behavior of rock bolts subjected to complex static and dynamic loads. Rock Mechanics and Rock Engineering 53: 4993-5004. https://doi.org/10.1007/s00603-020-02205-0.

Li, C.C. (2017). Rockbolting: Principles and Applications. Butterworth-Heinemann. https://doi.org/10.1016/B978-0-12-804401-8.00003-X.

Charette, F., Plouffe, M. (2008). A new rock bolt concept for underground excavations under high stress conditions. In Proceedings of the 6th International Symposium on Ground Support in Mining and Civil Engineering Construction, Johannesburg, South Africa, 225-240. http://www.saimm.org.za/Conferences/GroundSupport2008/225-240_Plouffe.pdf.

Sharifzadeh, M., Lou, J., Crompton, B. (2020b). Dynamic performance of energy-absorbing rockbolts based on laboratory test results, Part I: Evolution, deformation mechanisms, dynamic performance and classification. Tunnelling and Underground Space Technology 105: 103510. https://doi.org/10.1016/j.tust.2020.103510.

Li, C.C., Doucet, C. (2012). Performance of D-bolts under dynamic loading. Rock Mechanics and Rock Engineering 45: 193-204. https://doi.org/10.1007/s00603-011-0202-1.

Varden, R., Lachenicht, R., Player, J.R., Thompson, A., Villaescusa, E. (2008). Development and implementation of the Garford dynamic bolt at the Kanowna Belle Mine. In Proceedings of the 10th Underground Operators' Conference, Launceston, Australia, 95-104. https://www.researchgate.net/publication/265008457_Development_and_Implementation_of_the_Garford_Dynamic_Bolt_at_the_Kanowna_Belle_Mine.

Nguyen, B.V., Cai, M., Challagulla, K. (2019). Finite element analysis of the Superbolt under dynamic loading. In Proceedings of the Ninth International Symposium on Ground Support in Mining and Underground Construction, Perth, Australia, 375-386 https://doi.org/10.36487/ACG_rep/1925_25_Nguyen.

Marambio, E., Vallejos, J.A., Burgos, L., Gonzalez, C., Castro, L., Saure, J.P., Urzua, J. (2018). Numerical modelling of dynamic testing for rock reinforcement used in underground excavations. In Proceedings of the Fourth International Symposium on Block and Sublevel Caving, Perth, Australia, 767-780. https://doi.org/10.36487/ACG_rep/1815_60_Marambio.

John, S., C.M., Dillen, V., D.E. (1983). Rockbolts: a new numerical representation and its application in tunnel design. In Proceedings of the 24th U.S. Symposium on Rock Mechanics, College Station, USA, 13-25. https://doi.org/10.1016/0148-9062(84)91496-7.

Kang, H., Cui, Q., Wu, Z. (2014). Analysis on anchorage performances and affecting factors of resin bolts. Journal of China Coal Society 39, 1-10. https://doi.org/10.13225/j.cnki.jccs.2013.1919.

Zhao, X., Zhang, S., Zhu, Q., Li, H., Chen, G., Zhang, P. (2020). Dynamic and static analysis of a kind of novel J energy-releasing bolts. Geomatics, Natural Hazards and Risk 11: 2486-2508. https://doi.org/10.1080/19475705.2020.1833991.

Lou, J., Gao, F., Li, J., Yuan, G., Sharifzadeh, M. (2023). Effect of dynamic loading conditions on the dynamic performance of MP1 energy-absorbing rockbolts: Insight from laboratory drop test. International Journal of Mining Science and Technology, 33, 215-231. https://doi.org/10.1016/j.ijmst.2022.09.023.

Li, C.C., Hadjigeorgiou, J., Mikula, P., Knox, G., Darlington, B., Royer, R., Pytlik, A., Hosp, M. (2021). Performance of identical rockbolts tested on four dynamic testing rigs employing the direct impact method. Journal of Rock Mechanics and Geotechnical Engineering 13: 745-754. https://doi.org/10.1016/j.jrmge.2021.01.003.

Zhao, T., Zhang, Y., Li, C.C. (2021b). Radial stiffness of rock bolt samples and required thickness of the steel tube in impact tests. International Journal of Rock Mechanics and Mining Sciences 146: 104886. https://doi.org/10.1016/j.ijrmms.2021.104886.

Malvar, L.J., Crawford, J.E. (1998). Dynamic increase factors for steel reinforcing bars. In Proceedings of the 28th DDESB Seminar, Orlando, USA. https://www.researchgate.net/publication/235099732_Dynamic_Increase_Factors_for_Steel_Reinforcing_Bars

Si, L., Yang, J., Lou, J., Yuan, G. (2022). Deformation and stress characteristics of anchor bolt under axial impact. Journal of China Coal Society 47: 3645-3653. https://doi.org/10.13225/j.cnki.jccs.2022.0246.